Numerical Simulation of the
Hollow Cathode Discharge Plasma Dynamics

Ioannis G. Mikellides,[*] Ira Katz,[†] and Dan M. Goebel[‡]

Jet Propulsion Laboratory, California Institute of Technology, Pasadena, CA, 91109

Numerical simulations of a 1.5-cm diameter cathode used in the (25 kW$_e$) Nuclear Electric Xenon Ion System (NEXIS) have been performed to investigate the importance of ion acoustic turbulence and neutral gas viscosity in the orifice channel and keeper regions. These studies have been performed as part of the continued development and validation of the orificed hollow cathode code "OrCa2D" at JPL. The ultimate goal of the modeling effort is to develop a global model of the cathode plasma that can be used routinely to assess the life and performance of these devices. Simulations with an anomalously enhanced resistivity based on Sagdeev's effective collision frequency for ion acoustic turbulence show that the plasma potential and electron temperature increase by about 40% in the orifice/keeper region compared to the results obtained by using classical resistivity alone. Both plasma variables are closer to the measurement in this region when the anomalous contribution is added to the classical resistivity model. Based on the OrCa2D results for the heavy-species temperature in the NEXIS orifice channel (~1600 K), which is largely driven in this region by the channel wall temperature, the neutral gas Reynolds number is estimated to be on the order of unity. Thus, the OrCa2D neutral gas momentum equation has been updated to include the viscous terms. The preliminary simulations with viscosity show as much as 7× reduction of the axial velocity near the wall and a 3× reduction near the axis of symmetry compared to the inviscid solution. The steady state viscous solution for the total pressure inside the cathode (close to the inlet boundary) is 1.24 Torr compared to the measured value of 1.07 Torr. The previous inviscid solution continued to decrease with time below 0.4 Torr. The new results with viscosity also suggest however that the neutral flow transitions from the continuum to the rarefied regimes somewhere in (or close) to the orifice channel which would partially relax the no-slip boundary condition.

I.   Introduction

MANY missions considered under Project Prometheus would have required more than ten years of continuous thruster operation. The longest operation of a hollow cathode in an electric propulsion (EP) application was achieved during the Extended Life Test (ELT) of the NASA Solar Electric Propulsion Technology Applications Readiness (NSTAR) engine in which the discharge cathode continued to operate after 30,352 hrs.[1] However, the cathode keeper had completely eroded (Fig 1) and post-ELT analyses suggested that cathode failure would be the most likely near-term cause for the failure of the engine.[2] A detailed modeling effort, supported by a rigorous experimental investigation, was initiated in 2004 at JPL to assess the life of orificed hollow cathodes for high power electric propulsion like the 1.5-cm diameter cathode used in the Nuclear Electric Xenon Ion System (NEXIS).[3,4] The goal of the modeling effort has been to generate a global orificed cathode model that can predict accurately the evolution of the plasma in all regions of the cathode. The model could then be used to predict the life of the cathode and offer mitigating designs if needed. The physical laws that govern the evolution of the ionized and neutral gases

---

[*] Member Technical Staff, Advanced Propulsion Technology Group, 4800 Oak Grove Drive, Pasadena, CA, 91109, Mail Stop 125-109, Member AIAA.

[†] Group Supervisor, Advanced Propulsion Technology Group, 4800 Oak Grove Drive, Pasadena, CA, 91109, Mail Stop 125-109, Senior Member AIAA.

[‡] Section Staff, Thermal and Propulsion Engineering Section, 4800 Oak Grove Drive, Pasadena, CA, 91109, Mail Stop 125-109, Senior Member AIAA.

in these devices apply to cathodes of various sizes and operating conditions. Thus, although the models developed under this effort have been developed to support high-power EP for Project Prometheus (like the 25 kW$_e$ NEXIS), they can also be applied to discharge and neutralizer cathodes used in lower power EP like NSTAR (2.3 kW$_e$) and conventional Hall thrusters.

Fig 1. NSTAR hollow cathode at the beginning (left) and end (right, 30,352 hrs) of the Extended Life Test.

Two theoretical models have been developed to assess the life of orificed hollow cathodes. The first, a 2D-axisymmetric, time-independent code, dubbed IROrCa2D (Insert Region of an Orificed Cathode),[5,6] simulates the plasma inside the emitter region and thus depends on the measurement of at least one plasma property at the orifice entrance boundary. The second theoretical model, OrCa2D,[6] is a 2D-axisymmetric, time-dependent code that simulates the plasma and neutral gas dynamics in the emitter, orifice, keeper and plume regions and is more advanced than IROrCa2D in the physics and numerical approach. OrCa2D is self-reliant and thus does not depend on inputs from experimental measurements.

The first model, IROrCa2D, has been completed and has been benchmarked with detailed experimental data along the axis of symmetry of the NEXIS and NSTAR cathodes.[5,6] The model has been used to quantify the sheath drop and particle fluxes along the emitter. Contrary to previous expectations, which were based in part on the high discharge voltages observed during cathode operation, IROrCa2D predicted peak voltage drops along the emitting surface that did not exceed 8V (less than half the discharge voltage at the nominal operating condition of 25A and 5sccm). The computed magnitude of particle fluxes to the emitter, combined with a separate set of experiments at the University of California in San Diego (UCSD),[7] has led to the conclusion that the barium loss rate under the conditions inside the NEXIS hollow cathode is determined by thermal evaporation and is not enhanced as a result of the bombardment of the emitter by the plasma. As a result, cathode life may be modeled using vacuum cathode physics. Measurements of the insert temperature inside a smaller hollow cathode - the International Space Station (ISS) plasma contactor - provided information used to estimate the NEXIS cathode temperature, which provided the barium depletion time for a given cathode insert size from the cathode models. The temperature and the vacuum cathode depletion physics have been used in a simple model to estimate the cathode life for both dispenser and reservoir cathodes operating in a Prometheus1-class thruster.[8] The model predicts a life for the NEXIS cathode emitter that satisfies the requirement for Prometheus 1, i.e. >80 khrs. The simulations of the NSTAR cathode emitter region with IROrCa2D also suggested that emission is enhanced as the sheath along the insert becomes small enough to allow sheath penetration into the emitter pores thereby increasing the effective emission area.[6] The sheath size is reduced in the NSTAR cathode because it operates at much higher plasma peak densities (peak~10^{21} m^{-3}) than the NEXIS cathode (peak~10^{20} m^{-3}). *Without* emission enhancement physics the NSTAR cathode simulations suggest that the emitter would be utilized to a larger extent than the few millimeters presently shown by the simulations *with* enhancement.

The development of the second model, OrCa2D, continues. Although the majority of the physics have been implemented the code may not yet be used to accurately predict keeper erosion. The following work is required before OrCa2D may be used routinely to assess keeper erosion of different-size cathodes at various operating conditions: (1) incorporate keeper electrode boundary in the simulated geometry, (2) incorporate neutral gas collisional-to-rarefied transition physics, (3) incorporate ion dynamics, (4) improve computational speed by at least 4x, (5) complete validation with (existing) measurements. Despite the absence of the few remaining physics models in OrCa2D, several advancements in our understanding have been made with the present version of the code which are directly related to keeper erosion. For example, it is found that enhanced resistance resulting from two-streaming instabilities may be responsible for the high plasma potentials measured in the plume region. The hypothesis is based on the high e-i relative drifts calculated by OrCa2D in the near-plume region[6] and on the observed plasma oscillations captured in recent experiments.[9] Simulation of the plasma dynamics using the proper anomalous

2

resistivity model have been further pursued recently and the results are presented in this paper. Anomalous mechanisms and loss of collisionality between electrons in the plume region can lead to deviations from the Maxwellian electron energy distribution function (EEDF) and to "runaway" electrons, which would also support the presence of "primary" electrons in the discharge chamber of the ion engine. The significance of the finding on cathode life is that it may be possible to suppress plasma oscillations that produce high energy ions once the nature of the oscillation has been identified. For example, in the case of ion acoustic oscillations, wave damping may be achieved by increasing the ion temperature and/or elastic collisions with neutrals. The first may be achieved by increasing the temperature of surrounding boundaries like the keeper electrode. The second can be achieved by increasing the neutral gas density, either by direct injection from an external source or by modifications in the existing orifice plate/keeper geometry.

II.   Theoretical Models and Simulation Results

A. The OrCa2D codes

    The governing conservation laws and boundary conditions used in IROrCa2D and OrCa2D have been presented in detail by Mikellides, *et al.*[6] In summary, the codes solve an extensive system of conservation laws that is presently based on the global assumptions of quasi-neutrality (for the plasma) and continuum for all species. The latter fails in the plume region of the cathode, so continuum-to-rarefied transition physics are currently being implemented in the OrCa2D code. Both codes presently neglect the inertia terms in the electron and ion momentum equations. Collisions between electrons and neutrals (elastic and inelastic), electrons and ions and, ions and neutrals (charge-exchange) are included. Separate energy conservation equations are solved for the electron and heavy-species temperatures. Both ions and electrons are allowed to penetrate the sheath and be absorbed by the insert walls. Ions at wall boundaries are assumed to have attained the Bohm velocity. The electron current density absorbed by walls follows the one-sided thermal flux by assuming Boltzmann electrons. The emitted electron current density from the insert is modeled after the Richardson-Dushman equation for thermionic emission,[10] and includes the effect of the Schottky electric field. The emitter temperature as a function of distance from the downstream emitter edge is prescribed by a polynomial fit to measurements. Neutral gas dynamics are neglected in IROrCa2D ($u_n=0$) but are included in OrCa2D since the latter emulates the region downstream of the orifice entrance where the neutral gas inertia can become substantial. The system of eight (vector) equations in IROrCa2D along with appropriate boundary conditions yields the 2D profiles of the plasma particle density, ion and electron current densities, electric field, electron and heavy species temperature, neutral gas particle density and plasma potential. OrCa2D solves one additional conservation law, namely the neutral gas momentum equation, which yields the neutral gas flux. The regions of space simulated by each code are illustrated in Fig 2.

B. Numerical Simulations

Three major steps have been taken recently towards the completion of OrCa2D: 1) addition of anomalous resistivity in the plasma model, 2) addition of viscosity in the neutral gas model, and 3) addition of the keeper electrode in the NSTAR-simulated cathode. Each task has been completed independently of the other. For example, the most recent NEXIS simulation (presented herein) solves the full system of governing laws for the plasma and neutral gas, and includes the effects of viscosity in the latter; it does not however include the effects of anomalous resistivity. A different simulation of the NEXIS cathode (also presented in this paper) includes the effects of anomalous resistivity but is performed with a frozen neutral gas solution that did not include the effects of viscosity. The approach of excluding ("freezing") certain physics is customary when complex codes are employed to simulate complex problems because it helps identify the dominance of certain physical processes easier and with less computational resources. It also reduces the chance of miss interpreting numerical errors as real physics because it reduces the level of coupling between the various physical processes.

The results from the following NEXIS cathode simulations are presented in this paper:

- Case A: Plasma evolves to steady state with the neutral gas held frozen.
  - Plasma physics: classical+anomalous resistivity included.
  - Neutral gas physics: inviscid solution used (at p~1 Torr inside the cathode).
- Case B: Plasma and neutral gas evolve together to steady state.
  - Plasma physics: only classical resistivity included.
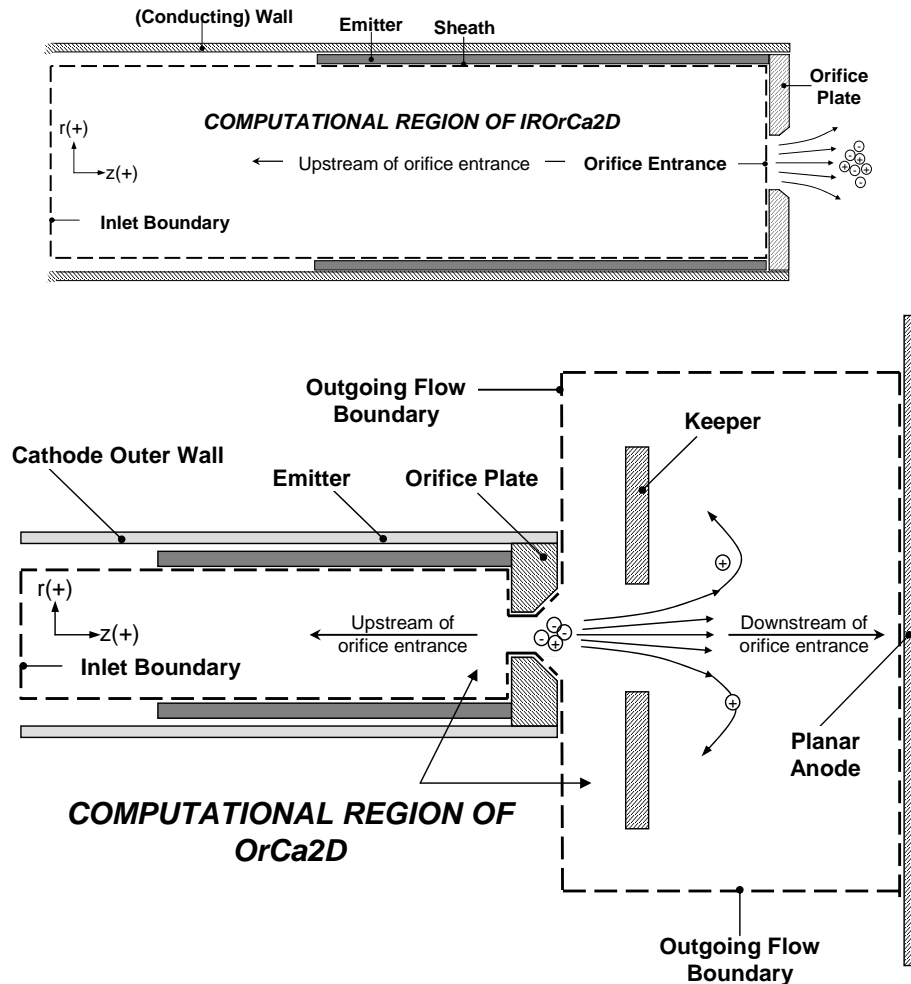 - Neutral gas physcis: viscosity included, transitional physics excluded.

Fig 2. Top: Schematic of the hollow cathode emitter region showing the IROrCa2D computational region (dashed line). Bottom: Schematic of the hollow cathode emitter, orifice and plume regions showing the OrCa2D computational region (dashed line).

The simulation cases A and B did not include the keeper electrode. However, much of the understanding gained through these simulations regarding the evolution of the plasma in the plume region is applicable both with and without the keeper. As explained above, it has been imperative to proceed in incremental steps towards the final hollow cathode model. Finally all simulations did not include the magnetic field. All comparisons presented in this report are made with data that also excluded the magnetic field.

1. Preliminary Assessments of Plasma Dynamics Using Anomalous Resistivity (Case A)
A main conclusion from the OrCa2D simulations of the NEXIS cathode, leading up to AIAA Paper 2005-4234,[6] was that the classical resistive contribution to the electric field in the near-plume region is not sufficiently larger (in magnitude) than the electron pressure gradient force to induce the large (time-averaged) plasma potential values measured in the experiment. The specific results of AIAA Paper 2005-4234 were produced by "freezing" the inviscid neutral gas solution at a time when the measured and computed total pressures were approximately equal inside the cathode (to about ~1 Torr). The plasma was then allowed to evolve accordingly. Based on those simulations it was postulated that enhanced resistance as a result of two-streaming instabilities may be responsible for the observed experimental trends. The hypothesis was based on the high e-i relative drifts calculated by OrCa2D in the near-plume region using classical transport, and on the observed plasma oscillations captured in recent experiments.[9] Anomalous mechanisms and loss of collisionality between electrons in the plume region may also lead to deviations from Maxwellian electron energy distribution functions (EEDF) in this region and to "runaway" electrons.

4

More specifically, the preliminary IROrCa2D simulations showed that up to the orifice entrance the electron Mach number M_e defined as the ratio of the relative e-i drift velocity u_d over $c_e=(kT_e/m_e)^{1/2}$ was less than about 0.2, where k is the Boltzmann constant, T_e is the electron temperature and m_e is the electron mass. As a consequence, only weak turbulence by ion-acoustic waves was proposed as the probable source of anomalous heating,[11] with an effective anomalous collision frequency first proposed by Sagdeev[12] (also in Hamberger and Friedman[13]) as follows:

$$\nu_{anom} \approx 10^{-2} \frac{\sqrt{\pi}}{8} \frac{T_e}{T_i} \frac{u_d}{c_e} \omega_e \qquad (1)$$

Using classical transport only, and the inviscid version of OrCa2D, it was shown in Ref. 6 that M_e exceeds seven in the near plume region (Fig 3, right). Buneman[14] (1959) showed that in this case it is possible to excite waves that have rapid growth rates. The Buneman wave frequency ω_B is,

$$\omega_B \approx \left(\frac{m_e}{16m}\right)^{1/3} \omega_e \qquad (2)$$

where ω_e is the electron plasma frequency. An effective anomalous collision frequency for the Buneman instability has been proposed by several authors and differs from the above by the specific (m_e/m) exponent. For example, Hamberger and Friedman[13] use 1/3 while other authors propose different exponents.[15,16] For comparison purposes Eqn (2) above is taken to be the representative anomalous collision frequency and the expected increase in the plasma resistivity due to the Buneman instability is estimated below. It is seen in Fig 3 that the enhancement can be as high as 50× under conditions that satisfy the Buneman criterion ($M_e \geq 1.3$), which could lead to significant heating of the electrons in the plume region. In view of the violent nature (short lifetime) of the Buneman instability, A. Treumann proposes that its effect is to "prepare" the plasma to become ion-acoustic-wave unstable by heating it to electron temperatures higher than the ion temperature, which would explain the recent ion-acoustic type of oscillations measured in the near-plume region of the NSTAR hollow cathode.[9]
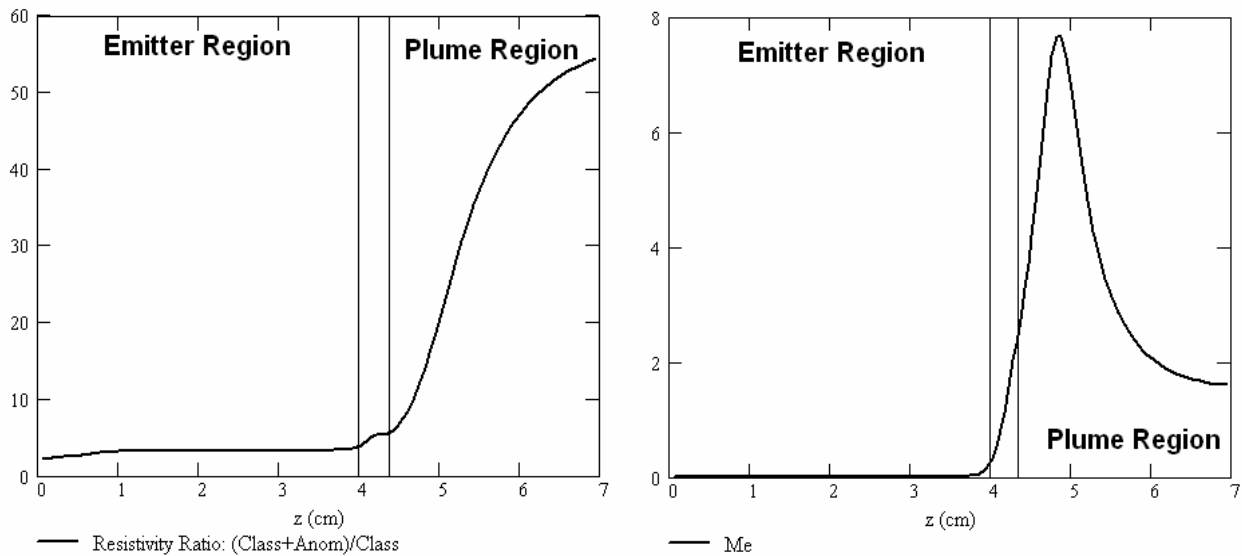

Fig 3. Left: Calculated resistivity enhancement using Buneman's wave frequency as the effective anomalous collision frequency. Right: Calculated electron Mach number M_e using classical resistivity only.

To investigate the possible transition from a Buneman-unstable to an ion-acoustic-unstable plasma, both anomalous resistivity formulae above were implemented in OrCa2D, namely Eqn. 1 when $M_e<1.3$ and Eqn. 2 when $M_e \geq 1.3$. With Sagdeev's formula alone it was not possible to obtain a steady state solution in the plume region; the Buneman frequency had to be implemented to slowly reduce M_e below unity in the near plume region (~4.2cm>z>5cm) before

the ion-acoustic mode could be effectively "turned-on." Although the observation supports the physical explanation of A. Treumann it does not yet establish concrete evidence of the Buneman-to-ion acoustic transition. Nevertheless, the combined implementation of the anomalous collision frequencies reduced M_e to values below about 0.1 in steady state, where only the ion-acoustic collision frequency (Eqn 1) was in effect (Fig 4, solid line).
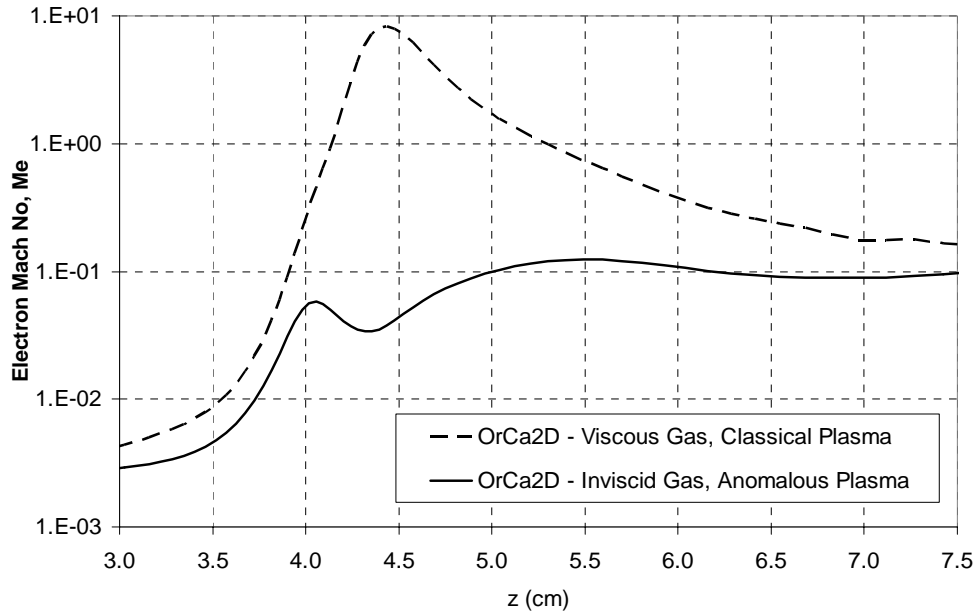

Fig 4. Electron Mach number (M_e) along the axis of symmetry of the NEXIS simulated cathode.

The simulations with the anomalous resistivity produced a significantly different behavior in the plasma compared to the results with classical resistivity. Specifically, Fig 5 shows a noticeable increase in the plasma potential in the plume region, as much 10V, close to the anode boundary. The axial profiles in Fig 6 show close agreement with the experimental values for the plasma potential up to the keeper electrode exit. The trend is also improved for the electron temperature (Fig 7). It is emphasized that the simulations presented here did *not* include the keeper electrode while all measurements were obtained *with* the keeper.

The impact of including a keeper electrode in the NEXIS cathode simulations has not yet been assessed. Two immediately obvious effects that are not included in the present results (as a consequence of excluding the keeper) are the expected neutral gas density changes in the keeper region, and the changes in the temperature of the heavy species. The first would directly affect the classical e-n collision frequency and the latter would enhance Sagdeev's anomalous collision frequency since the heavy species temperature is expected to be lower in this region as a result of the much colder keeper electrode. Although the changes in the neutral gas density can not be assessed without actually employing the keeper, a preliminary assessment of the impact of a colder surface on the heavy species temperature, and in turn on the anomalous resistivity, may be performed by implementing a "cold" boundary condition on the outer surface of the orifice plate. Based on visual observations of the "glow" of the keeper electrode during the operation of the NEXIS cathode, the outer surface of the orifice plate was set to 800K. The resulting heavy species temperature solution is compared with the previous solution in Fig 8. The previous solution was obtained using a value of 1453K for the boundary temperature. The effect of the colder surface on the anomalous plasma solution is shown in Fig 6 and Fig 7. As expected little to no change is observed in the plasma potential up to the keeper exit location (z=4.5cm) since the gas temperature in this region is set largely by the (warm) orifice plate. Farther downstream the plasma potential increases by as much as a few volts compared to the case with a warm boundary condition but continues to exhibit the same non-monotonic behavior away from the keeper exit. Negligible changes are observed in the electron temperature as a result of the colder neutral gas.

The 29ᵗʰ International Electric Propulsion Conference, Princeton University,
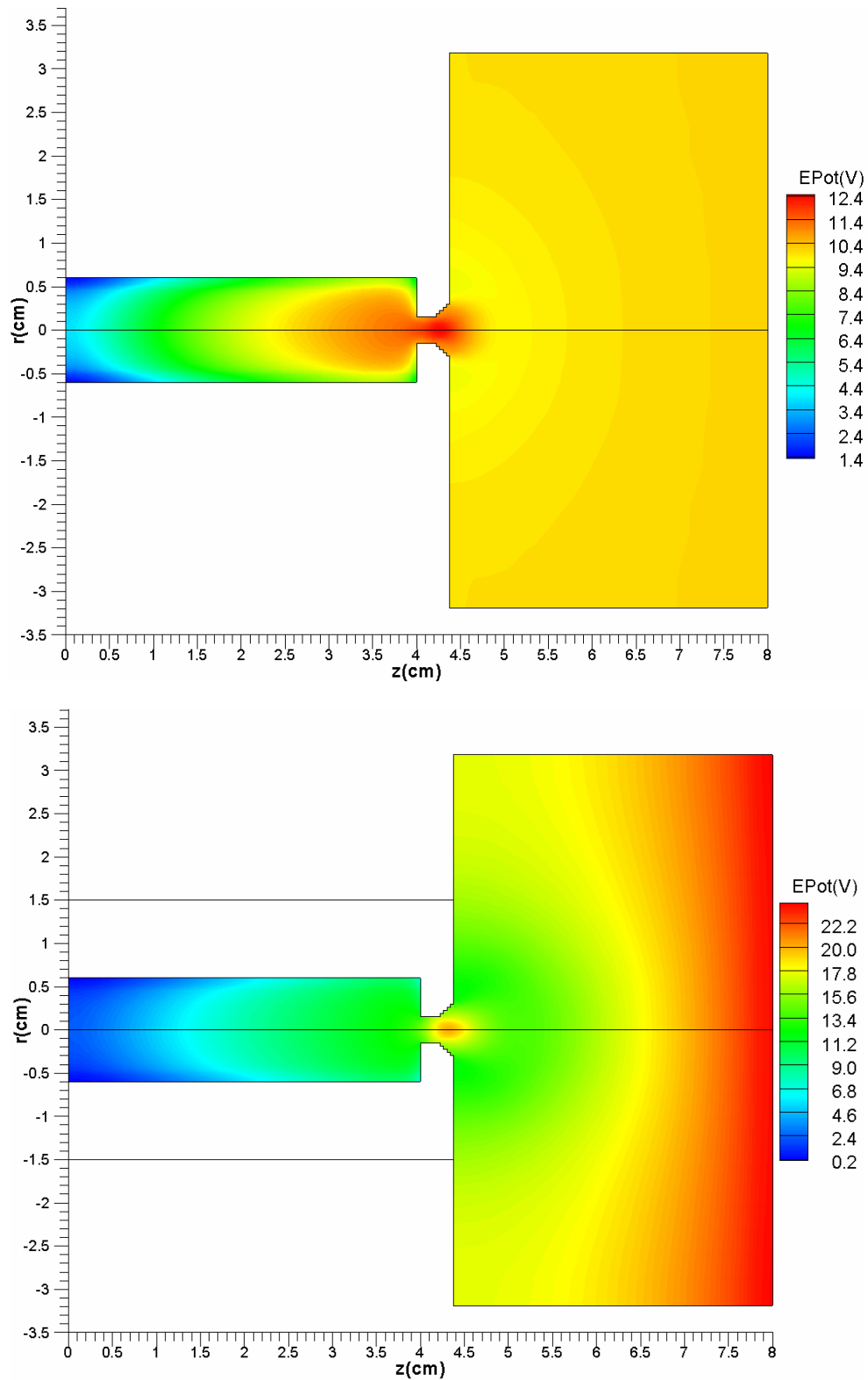*October 31 – November 4, 2005*

Fig 5. Computed plasma potential in the NEXIS simulated cathode (without a keeper). Case on top: Classical resistivity only with (frozen) inviscid neutral gas. Case on bottom: Classical+anomalous resistivity with (frozen) inviscid neutral gas.
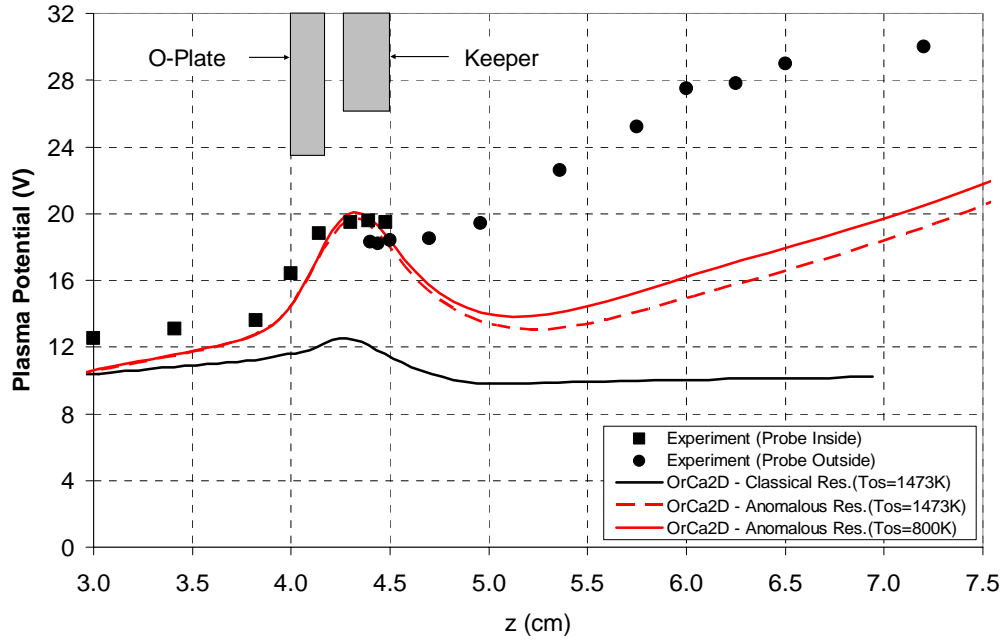
The 29ᵗʰ International Electric Propulsion Conference, Princeton University,
October 31 – November 4, 2005

Fig 6. Comparison between the measured and computed plasma potential along the axis of symmetry. (Note: The simulation results have not included the keeper electrode. The data have been obtained with the keeper electrode. "Tos" denotes temperature of the plate's outer surface.)
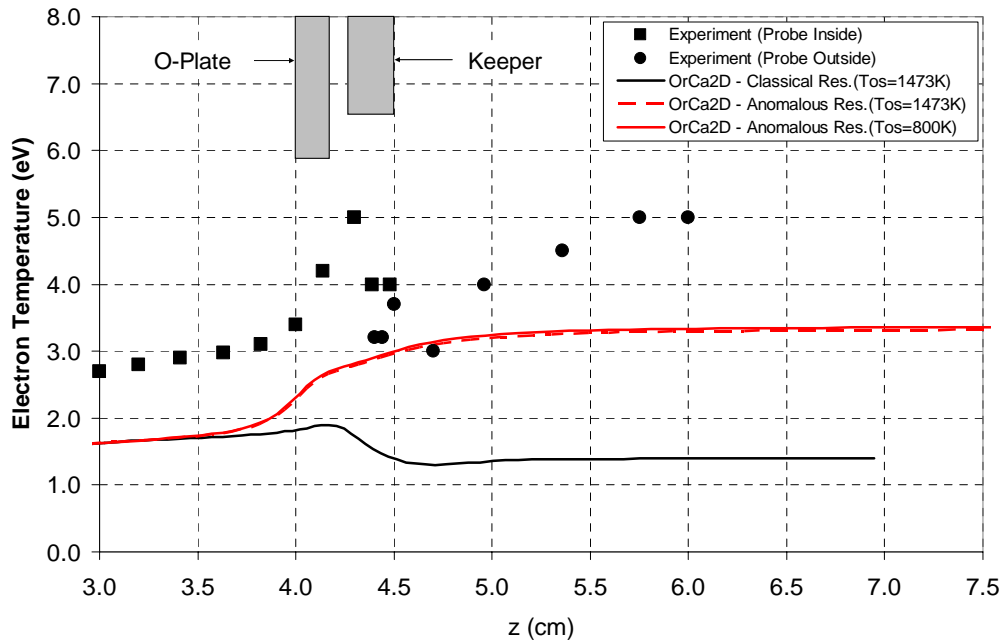
Fig 7. Comparison between the measured and computed electron temperature along the axis of symmetry. (Note: The simulation results have not included the keeper electrode. The data have been obtained with the keeper electrode. "Tos" denotes temperature of the plate's outer surface.)
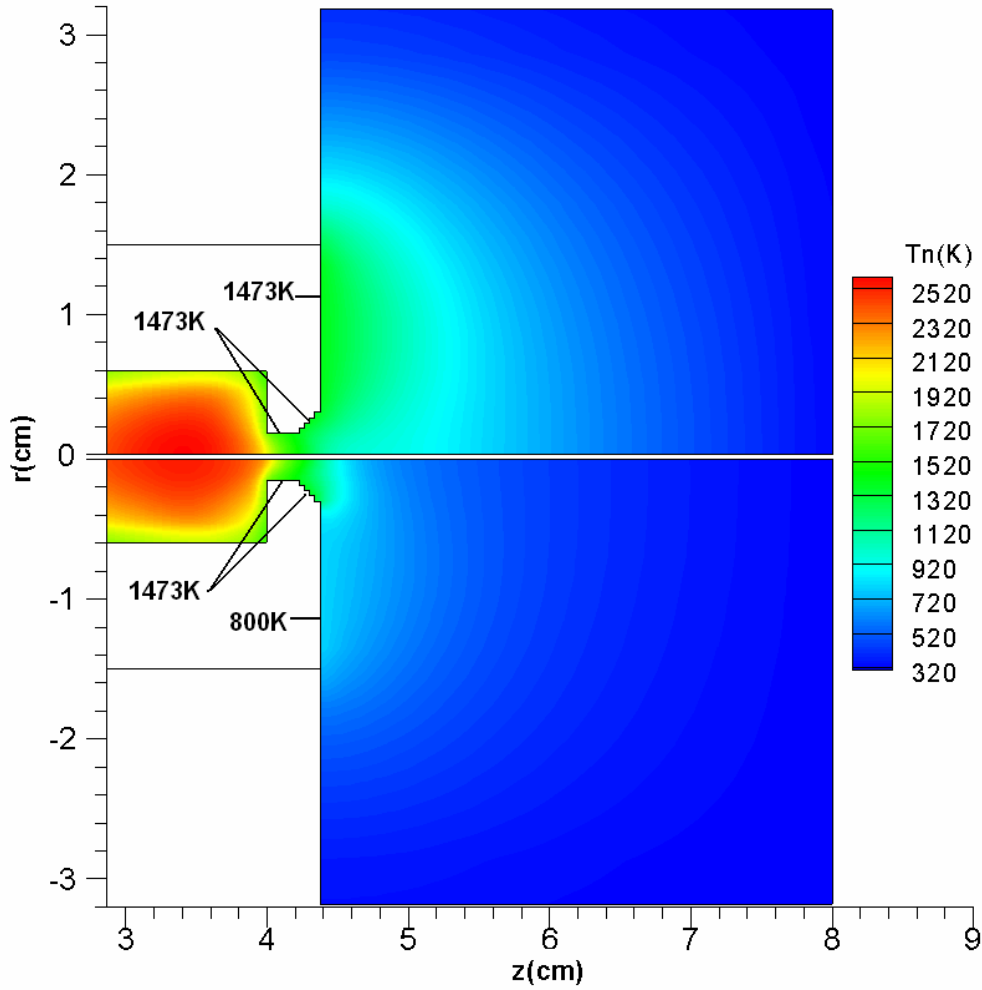
Fig 8. Neutral gas temperature with warm (top) and cold (bottom) outer orifice plate surface.

2. Neutral Gas Viscosity (Case B)

All simulations performed thus far have assumed that the neutral gas is inviscid. The inviscid solution yields supersonic flow in the orifice diverging section and plume regions. It was also found that under the inviscid assumption the total pressure inside the cathode continues to decrease below the measured value of about one Torr as shown in Fig 11 (left). An estimate of the Reynolds number inside the NEXIS and NSTAR-like cathodes operating at nominal conditions suggests that viscous effects are not negligible in the orifice channel, <u>under the continuum assumption</u>. For example, the Reynolds number Re in the orifice cylindrical section may be estimated as,

$$\mathrm{Re} \equiv \frac{\rho_n u_{n,z} L}{\mu} \approx \frac{\left(\dot{m}/\pi r_o^{\ 2}\right)L}{\mu} \tag{3}$$

where the viscosity coefficient μ is given by,[17]

$$\mu = 2.3 \times 10^{-5} \overline{T}^{(0.71+0.29/\overline{T})} \ \mathrm{Pa \cdot sec}, \qquad \overline{T}\left(\equiv T_{gas}/289.7\right) > 1 \tag{4}$$

and ρ_n is the mass density, $u_{n,z}$ is the axial gas velocity, $\dot{m}$ is the operating mass flow rate, r_o is the orifice radius and L is the length of the orifice channel. The Reynolds number as a function of the gas temperature is compared in Fig

9

9 for the two cathodes. At the calculated temperature of ~1600K in the NEXIS orifice channel, Re is about 0.8. To make an order-of-magnitude approximation of the boundary layer thickness δ we assume that the flow is laminar and that the channel is a flat plate. Then the Blasius solution (1908) would yield δ=5.2L/Re$^{1/2}$=4.36mm which is about 4× the channel radius. However, estimates of the Knudsen number in the orifice channel and plume regions[6] indicate that the neutral gas transitions from a collisional gas (inside the cathode) to a rarefied gas (in the plume), with transitional flow (Kn>~0.1-1) occurring mainly in the orifice channel region. As the continuum flow transitions into a rarefied gas it is well known that deviations from local thermodynamic equilibrium (LTE) invalidate the no-slip boundary condition and that, as the free-molecule flow regime is approached, the boundary layer looses its identity. It is therefore essential that transitional physics are included in this region; they have not been included in any of the modeling work that has been performed thus far. Also, by using the operating mass flow rate to compute Re, the contributions to the neutral gas flow of the ion flux to the walls that returns as neutrals and the loss of neutrals by ionization are not accounted for. Thus, the number 0.8 is only an order-of-magnitude estimate.

To perform a preliminary assessment of the effects of neutral gas viscosity we assume first that the continuum approximation prevails throughout the computational region. The partial failure of the assumption in the orifice channel implies that the continuum solution would overestimate the effects of viscosity in this region. For example, it is expected that the neutral gas velocity inside the orifice channel would be overly reduced because it would be calculated assuming a fully-developed viscous flow under the continuum assumption. In reality, as the flow transitions from continuum to rarefied, the "no-slip" boundary condition also relaxes to "slip." Thus, it is possible that in reality the sonic condition is in fact retained in the orifice channel; the flow is not expected to reach the sonic condition under the continuum assumption at Re=0.8.

The OrCa2D momentum equation (5) for the neutral gas has been augmented with the viscous terms, thereby making the code a Navier-Stokes solver. In the equations below, $\mathbf{\Gamma}_n$ is the neutral gas particle flux vector, n_n is the neutral particle density, T is the heavy-species temperature, $\mathbf{j}_i$ is the ion current density, and $\mathbf{u}_i$ is the ion velocity. The ion-neutral collision frequency and thermal conductivity are denoted by ν_{in} and κ_n, respectively. The complete set of governing laws for the neutral gas is shown below for completeness. The coefficients of viscosity λ and μ relate normal stresses to ∇·**u** and to the rates of extension respectively, and are (usually) related by the simple expression λ=-2/3μ (barred coefficients below denote values per unit mass). A no-slip boundary condition is implemented everywhere along wall boundaries including the orifice channel.

<u>Neutral Gas Governing Equations</u>

$$\frac{\partial \Gamma_{n,z}}{\partial t} + \nabla \cdot \left(\Gamma_{n,z}\mathbf{u}_n\right) = -\nabla_z\left(n_n kT\right)/m + n\nu_{in}\left(u_{i,z} - u_{n,z}\right) + \nabla_z\left(\overline{\lambda}\nabla \cdot \mathbf{u}_n\right) + \nabla \cdot \left[\overline{\mu}\left(\nabla_z\mathbf{u}_n + \nabla u_{n,z}\right)\right], \ \Gamma_{n,z} = n_n u_{n,z}$$

$$(5)$$

$$\frac{\partial \Gamma_{n,r}}{\partial t} + \nabla \cdot \left(\Gamma_{n,r}\mathbf{u}_n\right) = -\nabla_r\left(n_n kT\right)/m + n\nu_{in}\left(u_{i,r} - u_{n,r}\right) + \nabla_r\left(\overline{\lambda}\nabla \cdot \mathbf{u}_n\right) + \nabla \cdot \left[\overline{\mu}\left(\nabla_r\mathbf{u}_n + \nabla u_{n,r}\right)\right], \ \Gamma_{n,r} = n_n u_{n,r}$$

$$\frac{\partial n_n}{\partial t} + \nabla \cdot \mathbf{\Gamma}_n = -\dot{n} \tag{6}$$

$$\frac{3}{2}e(n_n + n)\frac{\partial T}{\partial t} = nm\nu_{in}\left(\mathbf{u}_i - \mathbf{u}_n\right)^2 - \nabla \cdot \left[\frac{3}{2}T\left(\mathbf{j}_i + e\mathbf{\Gamma}_n\right) - \kappa_n\nabla T\right] - eT\left[n\nabla \cdot \mathbf{u}_i + n_n\nabla \cdot \mathbf{u}_n\right] + \frac{3}{2}T\left[\nabla \cdot \left(\mathbf{j}_i + e\mathbf{\Gamma}_n\right)\right] \tag{7}$$

The evolution of the total pressure inside the cathode and inside the orifice channel (see theoretical probe locations in Fig 10) is shown in Fig 11. With the addition of viscosity it is now seen that the pressure close to the cathode inlet boundary is approximately 1.24 Torr which ~15% higher than the measured value. By comparison the value from the inviscid simulation was less than 0.5 Torr after 12ms and continued to drop (Fig 11, left). The effect of the boundary layer in the orifice channel is to reduce significantly the axial velocity of the gas as seen in Fig 12. Near the channel wall the velocity with viscosity is about 7× less than the value without viscosity. Near the axis of symmetry the reduction in velocity is 3×.
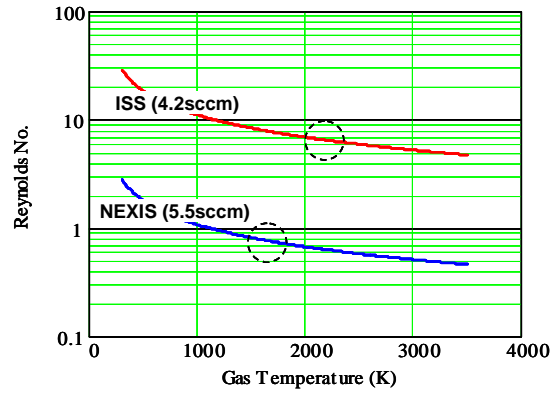
Fig 9. Reynolds number as a function of the neutral gas temperature in the orifice channel of the International Space Station (ISS) Plasma Contactor and NEXIS cathode.
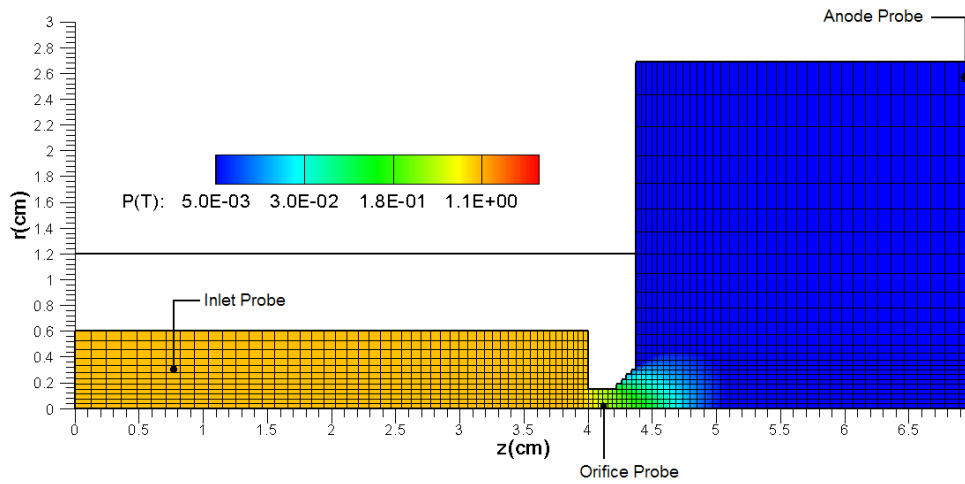

Fig 10. 2D profile of the total pressure for the NEXIS simulated cathode as computed by the inviscid OrCa2D at t=3ms.
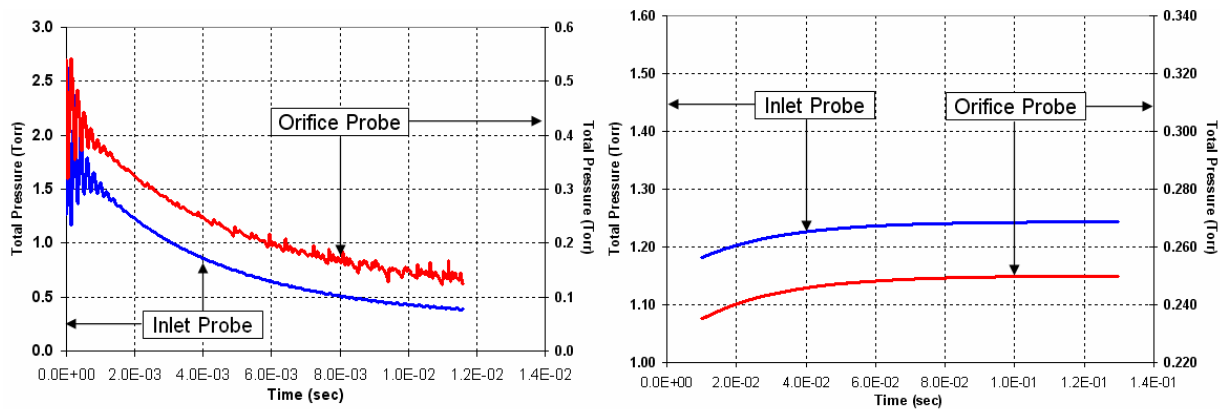

Fig 11. Total pressure as a function of time at different locations in the NEXIS simulated cathode. Left: Inviscid neutral gas. Right: Viscous neutral gas.

The 29th International Electric Propulsion Conference, Princeton University,
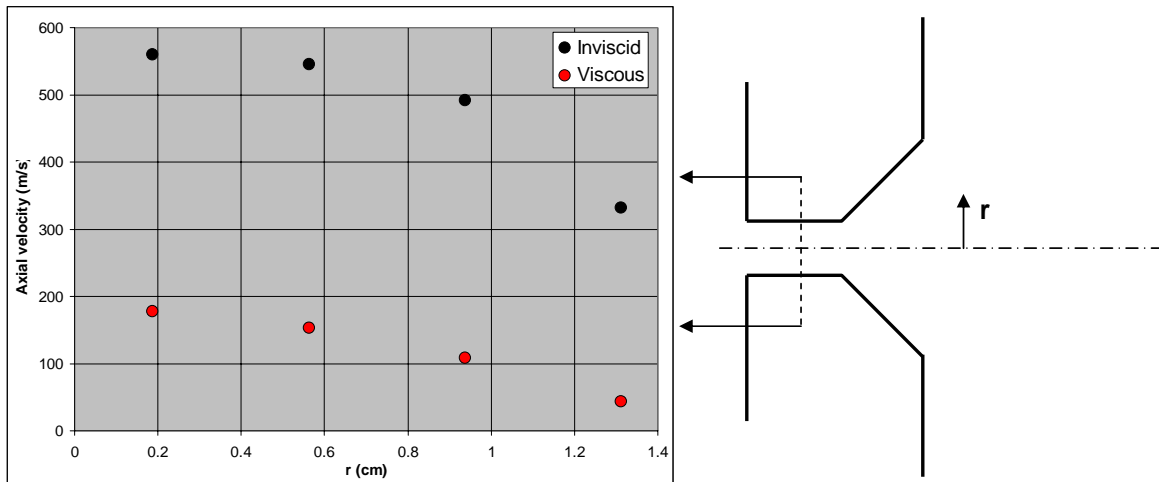*October 31 – November 4, 2005*

Fig 12. Comparison of the axial velocity component inside the orifice channel for the inviscid and viscous simulations.

The simulations with viscosity were executed *with* the plasma "turned on" as well. However, to extract the effects on the plasma of only the viscosity, no anomalous resistivity was implemented. Two effects on the plasma are immediately apparent as a consequence of viscosity. First, although the plasma potential in the near plume region is still considerably lower than the measurement, by comparison to the inviscid case (solid line) the potential exhibits an almost monotonic increase with distance from the orifice entrance. Second, the increase in electron temperature in the plume region is about as high as the increase seen in the inviscid case with anomalous resistivity. The results suggest that a combined simulation - viscous neutral gas plus anomalous resistivity - would produce an even better quantitative agreement with the experiment. The need for including anomalous physics in the simulation is further supported by Fig 4. It shows that with viscosity alone the electron Mach number continues to be supersonic as the plasma exits the orifice which is the condition for the excitement of two stream instabilities.

Cases A and B (see description in section B) are compared in Fig 15. The vector patterns in Fig 15 illustrate the formation of an (open) "ring" in the 2D plane that defines the location of electric field reversal. It is recognized that the existence of the ring is a direct consequence of the non-monotonic behavior of the plasma potential predicted by the code (see Fig 6), and is contrary to the measurement which exhibits no minima in the near-plume region. It is possible that the absence of specific physics and geometry features in the model (as described previously) is the reason for the discrepancy between the calculation and the measurement. In the presence of the experimentally observed oscillations, it is also possible that the plasma potential exhibits transient extrema that can not be resolved by the time-averaged measurement of Fig 6. The computed ring structure suggests that slow ions born near this ring would fall into it and be directed towards the electrode surface. This is supported by the radial velocity contours depicted in Fig 16 (left) which show that the highest ion energies are achieved at the location where the E-field ring intersects the outer plate surface. The contours are shown here for qualitative purposes only (thus the absence of a legend) since the exclusion of ion dynamics in the model does not yet allow for a quantitative assessment of ion energies. The exact radius of the ring and the ion energies depend on several physics including the location of the keeper, viscosity, anomalous resistivity and ion inertia. For example, in the absence of anomalous resistivity, Fig 15 (right) shows that the radius of the ring is reduced to such a size that any ions entering it would be directed towards the inside of the orifice channel rather than the outside electrode surface, as also suggested by Fig 16 (right). Therefore, in addition to anomalous resistivity, a complete model of the NEXIS cathode that can be used to assess accurately erosion and thus life of the keeper must also include the keeper, ion dynamics and transitional (continuum to rarefied) physics in the neutral gas.

The 29th International Electric Propulsion Conference, Princeton University,
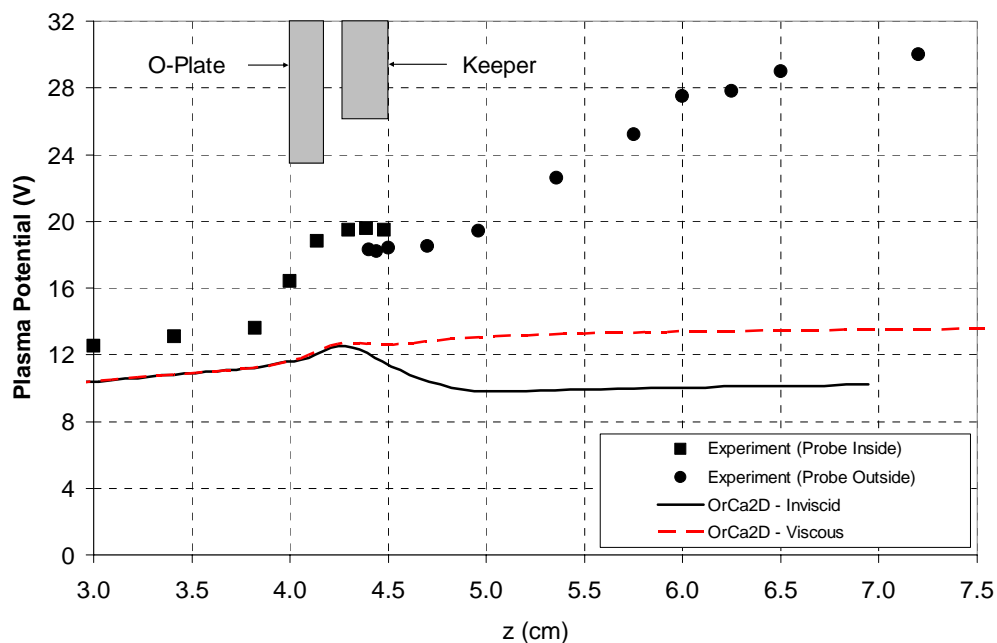*October 31 – November 4, 2005*

Fig 13. Comparison between the measured and computed plasma potential along the axis of symmetry. (Note: The simulation results have not included the keeper electrode. The data have been obtained with the keeper electrode.)
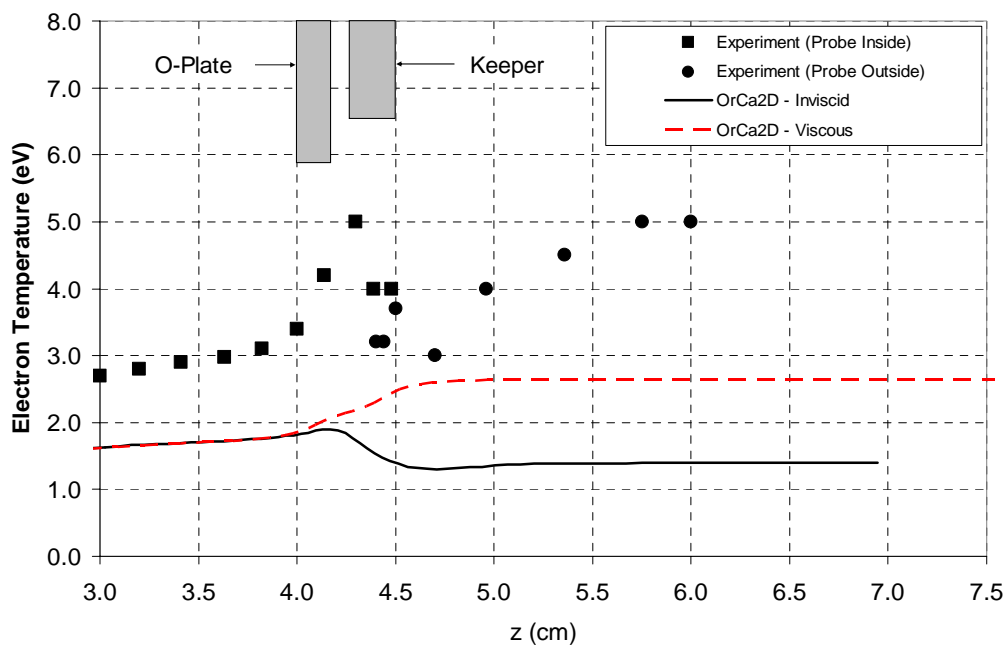

Fig 14. Comparison between the measured and computed plasma potential along the axis of symmetry. (Note: The simulation results have not included the keeper electrode. The data have been obtained with the keeper electrode.)
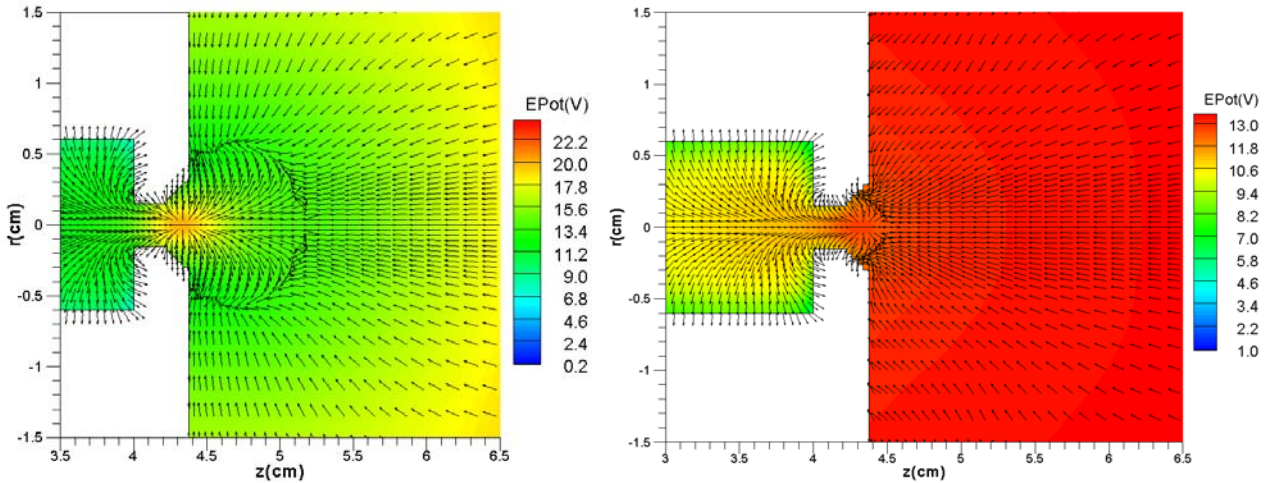
Fig 15. Direction of the electric field vectors in the vicinity of the orifice channel. Case (A) on the left: Plasma with anomalous resistivity, allowed to reach steady state in an inviscid neutral gas background that is "frozen" in time (at p~1Torr inside the cathode). Case (B) on the right: Plasma with classical resistivity coupled to a fully-viscous neutral gas in steady state.
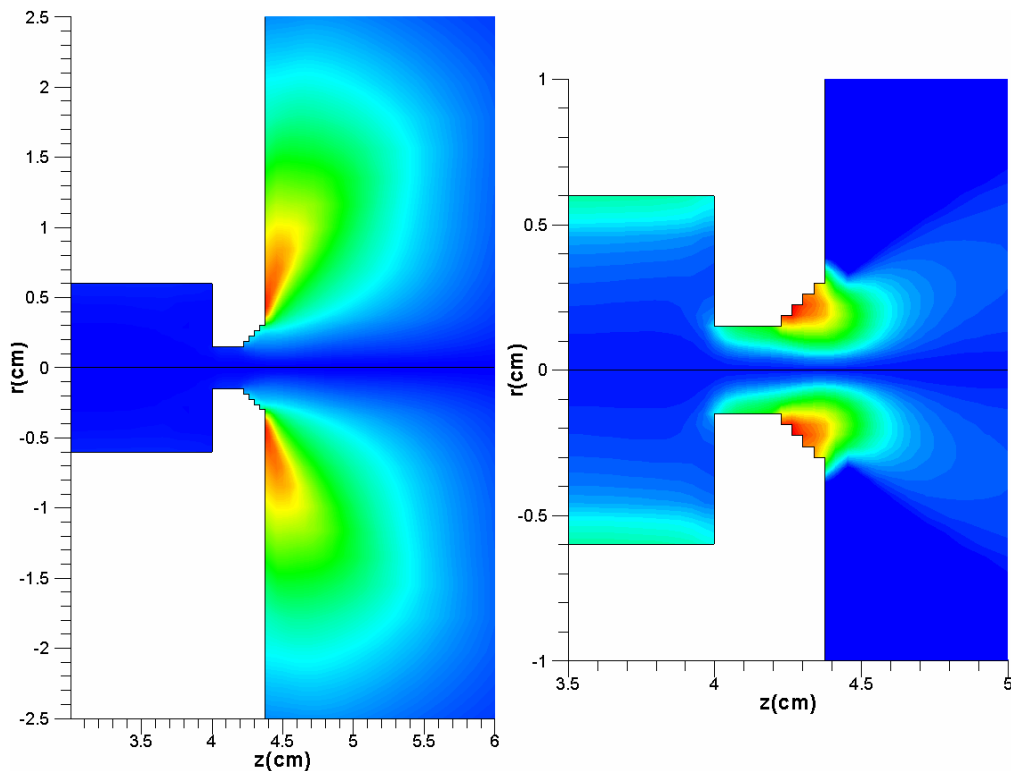

Fig 16. Ion radial velocity contours (shown for qualitative purposes) in the vicinity of the orifice channel. Case (A) on the left: Plasma with anomalous resistivity, allowed to reach steady state in an inviscid neutral gas background that is "frozen" in time (at p~1Torr inside the cathode). Case (B) on the right: Plasma with classical resistivity coupled to a fully-viscous neutral gas in steady state.

III.   Conclusions

Numerical simulations of the NEXIS hollow cathode plasma with an ion acoustic anomalous resistivity, in an inviscid neutral gas background, have shown that the plasma potential inside the orifice and keeper regions attains as much as 40% higher values than if classical resistivity alone is used. The results with anomalous resistivity are in excellent agreement with the measurement up to the keeper exit where the data exhibit a monotonic increase of the plasma potential with distance from the keeper exit. By contrast, approximately 0.75cm downstream of the keeper exit the calculations show a minimum in the plasma potential which defines the location where the electric field reverses direction. The non-monotonic behavior of the plasma potential in this near-plume region is a direct result of the competing resistive and pressure-gradient contributions to the electric field as dictated by Ohm's law. On the other hand, simulations using classical resistivity alone, in a viscous neutral gas, show an almost monotonic increase of the plasma potential beyond the keeper exit but to values substantially below the measurement. The relatively small increase of the plasma potential achieved as a result of viscous effects in the neutral gas is largely a result of the enhancements in the classical collision frequency between electrons and neutrals as the neutral gas flow is slowed down by as much as a factor of three along the axis of symmetry compared to the inviscid solution. The impact of the enhanced classical resistance in the plume region is found to be higher on the electron temperature than on the plasma potential. The simulation results from the two cases presented in this paper have advanced our understanding compared to previous work with the two OrCa codes by suggesting that both plasma wave motion (modeled here using ion acoustic anomalous resistivity) as well as viscous effects in the neutral gas are crucial drivers of the plasma evolution in the near plume region and consequently of the keeper life. A rigorous quantitative assessment and direct comparison with experimental data in this keeper region can only be performed once the keeper geometry, and all applicable physics have been coupled into a single numerical simulation.

Acknowledgments

References

[1] A. Sengupta, J. R. Brophy, and K. D. Goodfellow, AIAA Paper 03-4558, 39th AIAA/ASME/SAE/ASEE Joint Propulsion Conference, Huntsville, Alabama, 2003.

[2] A. Sengupta, *et al*., NASA T/TP 2004-213391, (2004).

[3] J. Polk, *et al*., AIAA-2003-4713, 39th AIAA/ASME/SAE/ASEE Joint Propulsion Conference, Huntsville, Alabama, 2003.

[4] T. Randolph and J. Polk, AIAA-2004-3450, 40th AIAA Joint Propulsion Conference, Fort Lauderdale, Florida, 2004.

[5] I.G. Mikellides, I. Katz, D. Goebel and J. Polk, AIAA Paper, 40th AIAA/ASME/SAE/ASEE Joint Propulsion Conference, Fort Lauderdale, Florida, 2004. (Updated version also accepted for publication in the *J. Appl. Phys.*)

[6] I.G. Mikellides, I. Katz, D. Goebel and J. Polk, AIAA Paper 05-4234, 41st AIAA/ASME/SAE/ASEE Joint Propulsion Conference, Tuscon, Arizona, 2005.

[7] R. Doerner, G.R. Tynan, E. Oyerzabal, K Taylor, D.M. Goebel, I. Katz, 40th AIAA/ASME/SAE/ASEE Joint Propulsion Conference, Fort Lauderdale, Florida, 2004.

[8] D. Goebel, *et al*., AIAA Paper 04-5911, Space 2004 Conference, San Diego, California, 2004.

[9] K. Jameson and D. Goebel, AIAA Paper 05-3667, 41st AIAA/ASME/SAE/ASEE Joint Propulsion Conference, Tucson, Arizona, 2005.

[10] S. Dushman, *Phys. Rev.*, **21**, 623 (1923).

[11] Stringer, T.E., *Plasma Physics, J. Nucl. Energy, Part C*, **6**, pp. 267-269, (1964).

[12] R. Z. Sagdeev, in *Proceedings of the 18th Symposium in Applied Mathematics*, p. 281, (1967).

[13] S. M. Hamberger and M. Friedman, *Phys. Rev.*, **21**, 674 (1968).

[14] O. Buneman, *Phys. Rev.*, **115**, 503 (1959).

[15] R. A. Treumann, Earth Planet Space, **53**, pp. 453-462 (2001).

[16] A. Hirose, *Plasma Physics*, 20, pp. 481-485, (1978).

[17] Reid, R.C., Prausnitz, J.M., and Sherwood, T.K., *The Properties of Gases and Liquids*, 3rd ed., McGraw-Hill, New York, 1977, pp. 402-403.

The 29th International Electric Propulsion Conference, Princeton University,
October 31 – November 4, 2005